



Role of the overriding plate in the subduction process: Insights from numerical models

Ylona van Dinther^{a,b,*}, Gabriele Morra^a, Francesca Funicello^a, Claudio Faccenna^a

^a Department of Geology, Università degli Studi 'Roma Tre', L.go S. Leonardo Murialdo 1, I-00146, Rome, Italy

^b Department of Earth Sciences, Utrecht University, Budapestlaan 4, 3584 CD Utrecht, The Netherlands

ARTICLE INFO

Article history:

Received 12 February 2009

Received in revised form 18 July 2009

Accepted 31 August 2009

Available online 10 September 2009

Keywords:

Subduction

Overriding plate

Subduction fault

Plate motion

Topography

Finite-element modeling

ABSTRACT

Active convergent margins are primarily shaped by the interplay among the subducting plate, overriding plate, and mantle. The effect of important forces, like far-field mantle flow, overriding plate motion, and inter-plate coupling, however, remains partially ambiguous. In a preliminary attempt to clarify their role, a self-consistent, viscoelastic, plane-strain, mechanical finite element model, in which subducting plate, overriding plate and mantle interact dynamically, is developed. In this quasi-static framework with a freely moving slab, trench, and inter-plate fault, the role of a compressive overriding plate on subduction zone kinematics, morphology and stress-state is characterized. A slab interacting solely with a semi-analytical three-dimensional mantle flow formulation shows that local non-induced mantle flow influences slab geometry and kinematics, adding an important dynamic term to the system. The impact of an overriding plate on this system is determined completely by overriding plate trench-ward motions and is only pertinent if the overriding plate actively advances the trench. A trench-ward moving overriding plate indents the slab and thereby enforces trench retreat and decreases slab dip. It also stimulates over-thrusting of the overriding plate onto the slab, and thereby permits mountain building within the overriding plate. Frictional resistance is observed to have a dominant local effect within the overriding plate as it is increasingly dragged down, thereby inhibiting the growth of overriding plate topography. A distinguishable effect on large-scale trench motions and deep slab dip is, however, absent for re-normalized friction coefficients ranging up to about 0.2. Minor additional effects include a decrease in plate motions of about 15% and slab bending stresses of about 10%.

© 2009 Elsevier B.V. All rights reserved.

1. Introduction

Subduction zones are intricate structures that dominate plate tectonics (e.g., Forsyth and Uyeda, 1975) and the appearance of the Earth. The main driving and resistive forces are reasonably well known. Negative buoyancy drives the slab down, while this is resisted by viscous mantle drag (e.g., Forsyth and Uyeda, 1975; Vlaar and Wortel, 1976; Chapple and Tullis, 1977). Uncertainty remains, though, concerning the role of other forces, such as bending resistance (e.g., Conrad and Hager, 1999; Schellart, 2004b; Buffet and Rowley, 2006), far-field mantle flow (e.g., Cross and Pilger, 1978; Zhong and Gurnis, 1995a,b), overriding plate motion (e.g., Jarrard, 1986; Lallemand et al., 2005; Heuret et al., 2007), and thrust inter-plate coupling (e.g., Conrad and Lithgow-Bertelloni, 2004). To increase the scientific understanding of these forces, which is vital for a more complete understanding of, e.g., seismogenesis, these last three forces are investigated in a self-consistent, buoyancy-driven subduction model.

The dynamics of subduction systems have been addressed by a number of modeling studies (for reviews, see Billen, 2008; Schmelting et al., 2008; Becker and Faccenna, 2009). Recently, slab dynamics is

often investigated using a simplified setup, where a freely subducting lithosphere interacts solely with a mantle (e.g., Jacoby and Schmelting, 1981; Kincaid and Olson, 1987; Funicello et al., 2003a; Schellart, 2004a; Bellahsen et al., 2005; Enns et al., 2005; Stegman et al., 2006; Royden and Husson, 2006; Capitanio et al., 2007). These models provide valuable insights in slab–mantle interaction, but the question remains; what is the impact of the missing overriding plate?

The overriding plate motion and structure is believed to be important for trench migration and slab geometry (Jarrard, 1986; McCaffrey, 1994; Lallemand et al., 2005; Heuret et al., 2007). Models that include a subducting and overriding plate, however, often lack a buoyancy-driven, free trench motion (e.g., Griffiths et al., 1995; Olbertz et al., 1997; Hassani et al., 1997), even though free trench migration is regularly included as well (e.g., Kincaid and Olson, 1987; Zhong and Gurnis, 1995a; Royden and Husson, 2006; de Franco et al., 2007). The introduction of an overriding plate also requires the definition of a plate contact, either as a narrow low strength zone, i.e., a subduction channel (e.g., Kapitzke, 1979; Babeyko and Sobolev, 2008; Gerya et al., 2008), or as discrete fault (e.g., Zhong and Gurnis, 1986; Kincaid and Sacks, 1997; Billen et al., 2003). The fault geometry is, however, often prescribed (e.g., Bott et al., 1989; Zhong et al., 1998; Krien and Fleitout, 2008).

This study investigates how subducting and overriding plate deformation may be linked and how the frictional characteristics of

* Corresponding author. Now at ETH Zürich, Institute of Geophysics, Sonneggstrasse 5, CH-8092 Zürich, Switzerland. Tel.: +41 44 632 3966; fax: +41 44 633 1065.

E-mail address: ylona.vandinther@tomo.ig.erdw.ethz.ch (Y. van Dinther).

the thrust fault and overriding plate motion influence this deformation. Although an exhaustive study is still necessary, it will be shown how the proposed numerical methodology enables modeling that captures both large-scale and smaller-scale dynamics. The first section sets benchmarks for the single slab evolution and investigates the role of varying mantle flow pressures beneath the trench. In the second part, an overriding plate is added to characterize its role and the interaction between slab and overriding plate in a free-trench, freely evolving fault subduction system.

The buoyancy-driven approach with a Coulomb frictional fault, as is adopted in this study, shows that the influence of an overriding plate is only distinct if the overriding plate actively advances toward the trench. Furthermore, it is evident that the role of frictional resistance, for a friction coefficient up to about 0.2, is negligible on a regional to global scale, but does affect local overriding plate geometry and stresses significantly. Although minor changes in plate motions (+15%) and slab bending stresses (−10%) can be observed. Finally, it is observed that mountain building on the overriding plate requires trench-ward overriding plate motion, and is negatively correlated with inter-plate friction.

2. Numerical modeling approach

In this study, a two-dimensional implicit mechanical Lagrangian finite element model is employed (Fig. 1). The plane-strain subducting and overriding plates interact with a mantle flow in which the third-dimensional toroidal- and poloidal components are roughly captured by a set of horizontal and vertical drag forces. This self-consistent, internally-driven approach is based on Funiello et al. (2003b) and Morra and Regenauer-Lieb (2006a,b) and has been successfully employed by Capitanio et al. (2007) and Goes et al. (2008). This solid mechanical model with fluid mantle flow feedback circumvents problems related to either a pure fluid-dynamic approach or an isolated quasi-static solid-mechanical approach (Morra and Regenauer-Lieb, 2006a) and allows for a detailed quantification of energy and stresses. The mechanical conservation equations, i.e., the conservation of mass and momentum, are solved

using the commercial finite element package ABAQUS™ Standard (Hibbit et al., 2007).

2.1. Model setup

The model setup is shown in Fig. 1, while related model parameters are described in Tables 1 and 2. The inherent simplicity of the adopted generic setup was chosen to provide insight into general physical processes at work rather than to reproduce specific natural cases. Initiation of subduction is accomplished through a vertically downward body force of $3 \cdot 10^4 \text{ N} \cdot \text{m}^{-2}$, which increases until a depth of 100 km over an area of 150 km for a maximum time of 3.16 My. This condition allows the body forces to overcome resistive forces, thereafter triggering a self-sustained subduction (e.g., Faccenna et al., 1999; Hall et al., 2003; Gurnis et al., 2004).

The detailed setup of each model component, which refers to a subducting plate, overriding plate, lithosphere–mantle interaction and inter-plate fault characterization, is provided in Appendices A–D, respectively. The investigated parameters in: a) single subducting plate models, and b) subducting and overriding plate models are summarized in Table 3.

3. Results

3.1. Single subducting plate

The objective of this set of experiments is two-fold, a) to benchmark the model setup, and b) to establish the role of a variational mantle flow pressure beneath the trench (W), resulting from a variation of in slab width (Dvorkin et al., 1993) and other non-induced, external mantle flow sources (Nelson and Temple, 1972). To define important parameters influencing slab dynamics, three additional parameters are investigated: a) slab buoyancy or slab–upper mantle density contrast (DR), b) slab–upper mantle viscosity contrast (Iso), and c) ridge push (RP) (Table 3).

The evolution of a single subducting lithosphere (Fig. 2) in terms of subduction velocities (Fig. 3, see Fig. 1 for definitions) depicts three

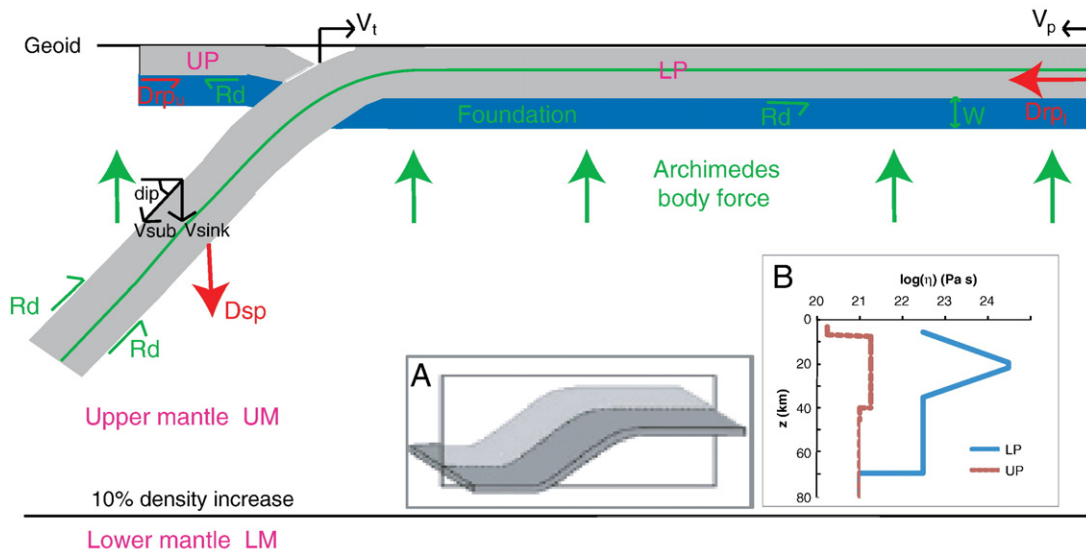


Fig. 1. Model setup showing subduction system geometry including driving forces in red, slab pull D_{sp} and ridge push D_{rp} , and opposing forces in green, mantle drag R_d , Archimedes body force A_r and a foundation. Dash pots representing mantle drag are located at the green lines; at the strongest part for the downgoing plate and at the bottom for the overriding plate. The Archimedes body force compensates for the physical absence of a mantle (ρ_m, g) and is applied until *Geoid*, the imposed sea level, for both lithospheres (*LP* and *UP*). The blue foundation area, applied over a depth extent W , represents both an isostatic contribution and an additional mantle flow pressure variation. Definitions and conventions for kinematic parameters are added in black: trench retreat velocity v_t , plate advance velocity v_p , subduction velocity v_{sub} , sinking velocity v_{sink} and deep slab dip α . Insets show: (A) Modeled section in three dimensional perspective as represented by 3-D mantle flow calculation of drag forces, and (B) Viscosity profiles for subducting lithosphere (*LP*) and overriding lithosphere (*UP*). Inspired by Capitanio et al. (2007).

Table 1

Model parameters for each component; subducting plate, overriding plate, and upper mantle. These reference values are used unless otherwise specified.

Parameter	Symbol	Unit	Subducting (LP)	Overriding (UP)	Mantle (UM)
Dimensions	$h_x/L_x/w_x$	km	70/1800/1000	40/230/1000	Unbounded
Density ^a	ρ_x	$\text{kg}\cdot\text{m}^{-3}$	3300	3300	3220
Viscosity	η_x	Pa·s	$6.5 \cdot 10^{23b}$	$2.7 \cdot 10^{21b}$	$1 \cdot 10^{21}$

^a Applied densities are relative to $2600 \text{ kg}\cdot\text{m}^{-3}$.

^b Average values. See profiles.

Table 2

General model parameters. These reference values are used unless otherwise specified.

Parameter	Symbol	Value	Unit
Viscosity lower mantle	η_{lm}	η_m	Pa·s
Density lower mantle ^a	ρ_{lm}	$1.1 \cdot \rho_{um}$	$\text{kg}\cdot\text{m}^{-3}$
Density water ^a	ρ_w	1000	$\text{kg}\cdot\text{m}^{-3}$
Young's modulus	E	$2 \cdot 10^{11}$	Pa
Poisson's ratio	ν	0.3	–
Gravity	g	9.8	$\text{m}\cdot\text{s}^{-2}$

^a Applied densities are relative to $2600 \text{ kg}\cdot\text{m}^{-3}$.

distinct phases (e.g., Funicello et al., 2003a). Over time, a progressive increase in both trench and plate velocities is observed (Fig. 3a,b), as a larger part of the slab falls freely into the mantle (Phase 1, Fig. 2a). Steady state kinematic conditions (Phase 3, Fig. 2c–e) are reached 2–3 Myrs after the slabs interaction with the 660 km discontinuity (Phase 2, Fig. 2b).

3.1.1. Oceanic corner flow pressure

Mantle flow pressure below the trench, parameterized by a foundation extending over a variable depth W , is an important parameter affecting both subduction velocities and slab geometry (Fig. 3). Smaller additional flow pressures, equivalent to a smaller slab width or smaller far-field mantle flow, result in increasingly higher trench retreat rates (Figs. 3a and 4a) and higher plate velocities (Figs. 3b and 4b). Plate velocities show a minimum rate of about $1 \text{ cm}\cdot\text{yr}^{-1}$. Furthermore, the relative importance of plate versus trench motion, v_p/v_t , increases with increasing flow pressure (Figs. 3 and 4).

Trench advance can be observed for models $W=30$, $W=25$ & $DR=40$, $W=25$ & $DR=60$, and $W=20$ & $DR=40$ (Figs. 3a and 4a). In these models, trench advance rates are in the order of magnitude of plate motions (Fig. 3a,b), so, effectively, subduction is stalling. Therefore, these models are deemed non-viable.

Total subduction velocities, $v_{\text{sub}} = v_t + v_p$ (for definitions see Fig. 1), and sinking velocities, $v_{\text{sink}} = v_{\text{sub}} \cdot \cos(\alpha)$, show results similar to those for trench retreat, as trench retreat is the dominant mechanism of

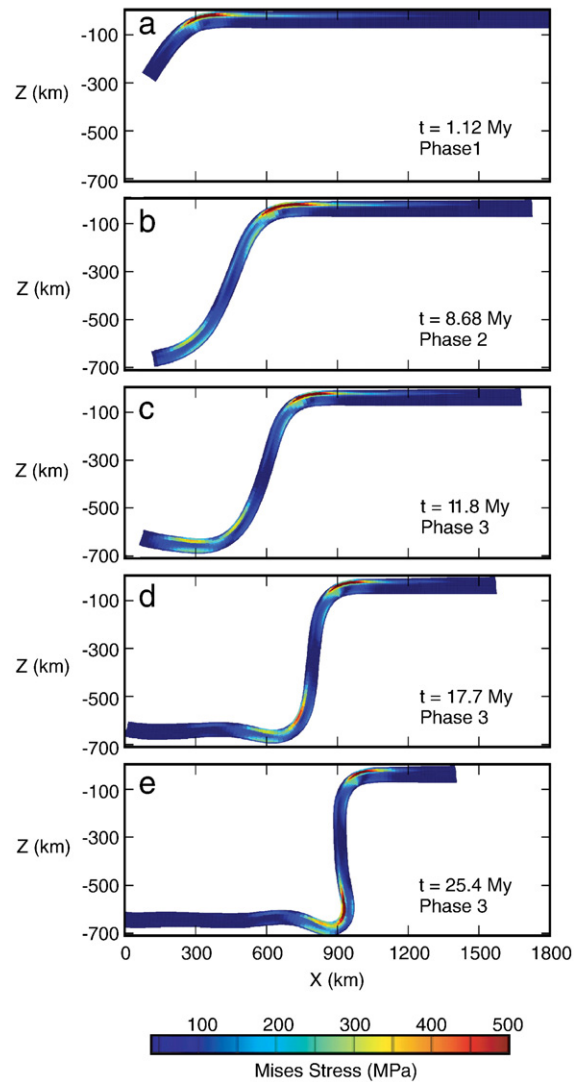


Fig. 2. Evolution of a single subducting plate over time depicting different subduction phases, while showing Mises stress. X is distance relative to the original single slab starting point and Z is depth relative to imposed geoid or sea level.

subduction. Sinking velocities can be compared to the Stokes velocity of a sinking squared plate (dash-dotted lines for different density contrasts), $v_{\text{stokes}} = \frac{hL\delta\rho g}{12\sqrt{2}\eta}$, where h is lithosphere thickness, L is free length of the slab within the mantle, and $\delta\rho$ is density contrast between oceanic lithosphere and upper mantle (Capitanio et al., 2007). This comparison

Table 3

Investigated parameters.

Parameter	Abbreviation	Unit	Min. value	Max. value	Interm. values
<i>Subducting plate</i>					
Depth extent restoring force	W	km	10	30	15,20,25
Density contrast	DR	$\text{kg}\cdot\text{m}^{-3}$	40	80	60
Slab viscosity	iso	Pa·s	$1.0 \cdot 10^{22}$	$1.0 \cdot 10^{24}$	$1.0 \cdot 10^{23}$
Ridge push subducting plate	RP_p	$\text{N}\cdot\text{m}^{-1}$	0	$3 \cdot 10^{12}$	–
<i>Subducting and overriding plate</i>					
Density contrast	DR	$\text{kg}\cdot\text{m}^{-3}$	60	80	–
Inter-plate friction	F_{UL}	–	0.0	1.0	0.1,0.2,0.3,0.5,0.7
Traction UP for DR80	T_{60}	$\text{N}\cdot\text{m}^{-1}$	$2.2 \cdot 10^{12}$	$9.4 \cdot 10^{12}$	$5.8 \cdot 10^{12}$
Traction UP for DR60	T_{80}	$\text{N}\cdot\text{m}^{-1}$	$7.2 \cdot 10^{10}$	$1.4 \cdot 10^{13}$	$7.2 \cdot 10^{11}$, $5.0 \cdot 10^{12}$
Viscosity overriding plate	$UP \text{ vis}$	Pa·s	$2.7 \cdot 10^{21}$	$9 \cdot 10^{22}$	–

Numbers are used in combination with abbreviations to form a model name. Viscosities are averaged viscosities if required. Reference parameters are depicted in red.

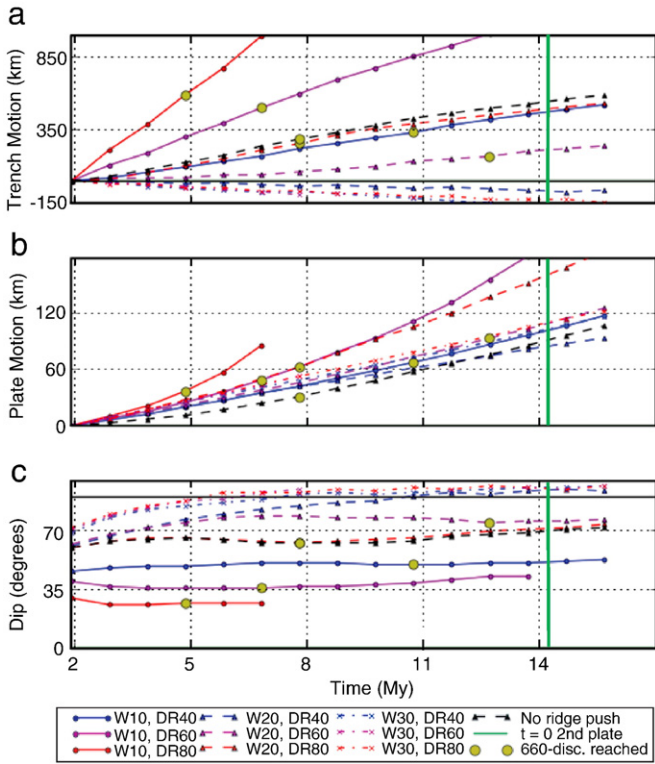


Fig. 3. (a) Amount of trench motion, (b) amount of subducting plate motion, and (c) slab dip angle evolving over time for a single subducting plate. Different line styles indicate different depth extents of the foundation and different colors indicate different slab–upper mantle density contrasts. For comparison, a black dashed line for an absent ridge push for the subducting plate is added. Markers show times of measurement of the parameters. Yellow dots indicate the time at which the slab reached the 660 km-discontinuity. The green vertical line indicates the moment at which the overriding plate is included in the next set of models, as parameters are assumed to be in steady-state from that line forward. A trench location where the top of the subducting plate reaches a depth of 25 km is assumed. Both slab pull and a variation in mantle flow pressure dramatically influence slab dynamics.

shows that sinking velocities are increasingly lower than Stokes velocity for foundations larger than 8 km.

The morphology of subduction models can be unambiguously expressed in terms of deep slab dip ($100 < z < 300$ km, Fig. 3c). Steady-state dips, which are reached after about 8 My, are about 28° – 35° – 50° for decreasing density contrasts of $W=10$, about 65° – 75° – 92° for $W=20$, and sub-vertical for $W=30$ (Fig. 3c). This shows that higher trench and plate velocities correspond to shallower dips.

3.1.2. Slab–upper mantle viscosity contrast

Slab dynamics are sensitive to viscosity contrast (yellow, white, and green dots in Fig. 4). Increasing viscosity contrast by one order of magnitude to about $1.0 \cdot 10^{24}$ Pa·s results in an increase of about 120% in trench retreat and about 30% in plate motion (Fig. 4). These velocity increases lead to an accompanying decrease in slab dip from 65° to 39° . A one order of magnitude decrease in constant viscosity results in a decrease of 24% in trench retreat and 71% in plate motion.

3.1.3. Ridge push

The influence of ridge push on slab motions is evaluated by comparing the reference model with ridge push (dashed red line) to a model without ridge push (black dashed line) in Fig. 3. The latter shows a negligible increase in trench retreat, 42% decrease in plate motion, and, again, a negligible decrease in slab dip.

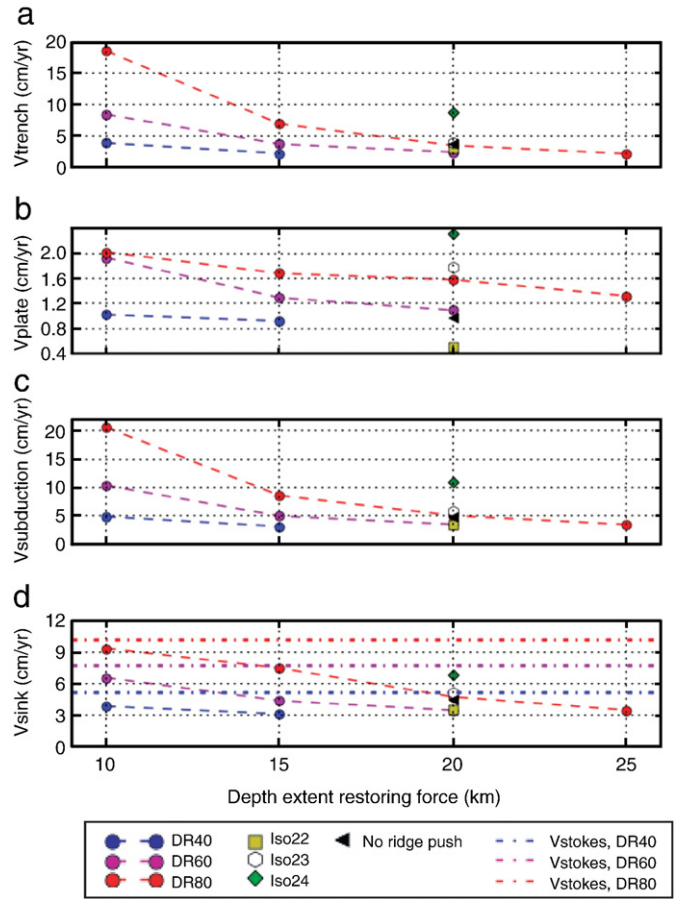


Fig. 4. Absolute average steady-state velocities in a single slab subduction system in $\text{cm}\cdot\text{yr}^{-1}$ for all viable models. (a) v_t , trench velocity, (b) v_p , plate velocity, (c) v_{sub} , total subduction velocity, and (d) v_{sink} , vertical sinking velocity. Dotted lines indicate different slab–upper mantle density contrasts (DR), yellow, white and green dots shows different constant slab viscosities of resp. $\eta_{\text{lith}} = 1 \cdot 10^{22}$ Pa·s, $\eta_{\text{lith}} = 1 \cdot 10^{23}$ Pa·s, and $\eta_{\text{lith}} = 1 \cdot 10^{24}$ Pa·s. Black triangle depicts a model without ridge push. The analytically calculated Stokes velocity, using reference parameters, is shown as a dashed-dotted line in panel d. Stronger slabs subduct faster.

3.2. Subducting and overriding plates

The interaction between the subducting and overriding plate is investigated using a compressive overriding plate regime for four potentially important parameters; a) slab pull (through density contrast DR), b) inter-plate fault friction (FUL), c) overriding plate traction or relative trench-ward motion (T), and d) overriding plate strength (UP vis) (Table 3). The inter-plate friction coefficients of 0.0 to 1.0 mentioned throughout this study correspond to actual, re-normalized friction coefficients of $O(0.02)$ – $O(0.2)$ (see Section 4.2).

A close-up of diagrams for differing inter-plate friction and slab buoyancy shows qualitatively that slab characteristics, in terms of trench retreat and bending stresses, are hardly affected by inter-plate friction (Fig. 5). However, it is observed that overriding plate geometry and stresses are affected considerably.

Overriding plate motions are controlled by a traction applied below the overriding plate, representing the sum of contributions from induced arc corner flow, ridge push and other far-field forces. A first order estimate of an appropriate range of overriding plate traction in a two plate configuration (Table 4) is made based on two criteria. For the lower boundary, the overriding and subducting plates should attach completely. For the upper boundary, they should not cause unrealistically high trench retreat velocities (Fig. 6a,b) or lead to an increasing overriding plate topography away from the trench (Fig. 7b, yellow line).

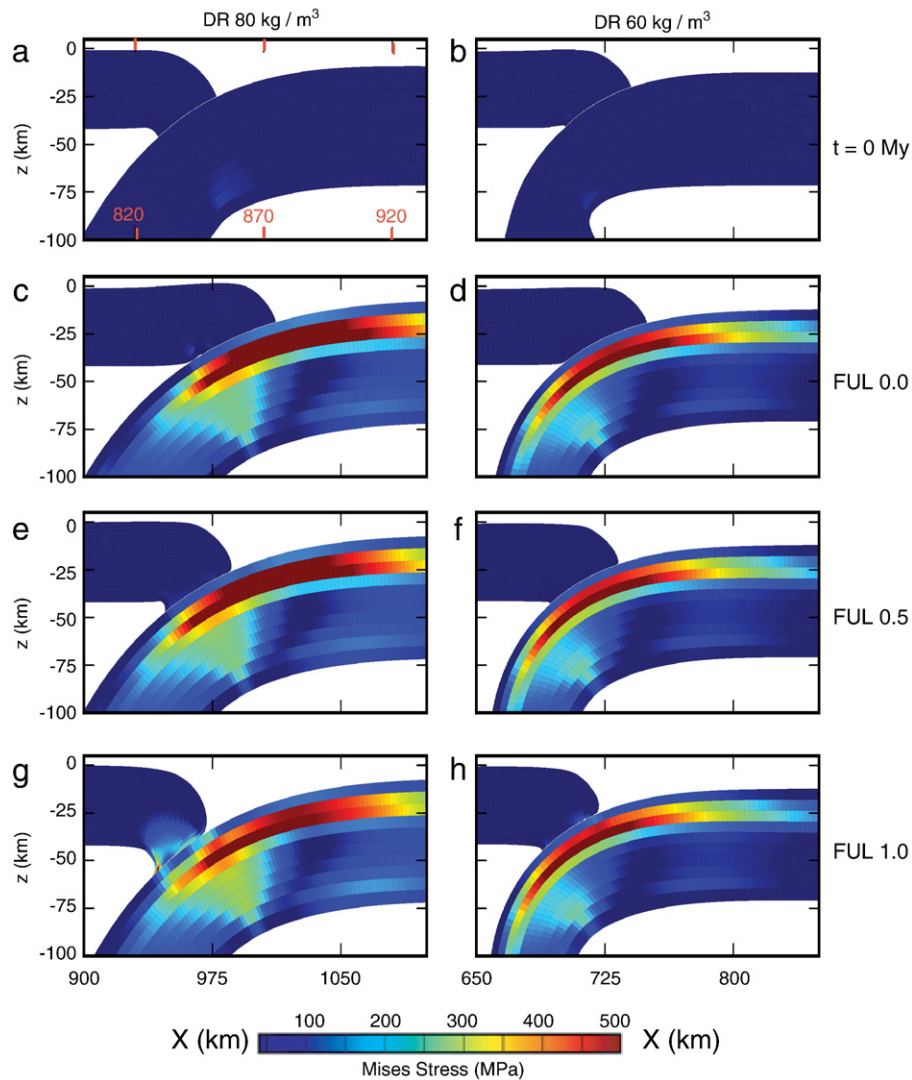


Fig. 5. Subducting and overriding plate contact region for a wide range of inter-plate frictions (rows) and density contrasts (columns) at $t_{TP} = 6.65$ My. Top panels show the initial configuration. Note different red X coordinates for the starting configuration of DR80. Actual inter-plate shear stress is shown in Fig. 11. Inter-plate friction affects overriding plate topography and stresses significantly.

To make a proper distinction between different types of behavior, the term passive traction is introduced here. Passive traction is defined as the forcing for which the overriding plate push does not affect slab kinematics. Estimates of passive traction values (Table 4) show that DR80-models have a reference traction value that is larger than that of passive traction (+164% according to $\frac{\text{Reference} - \text{Passive}}{\text{Passive}} \cdot 100\%$), which results in a compressive overriding plate regime. DR60-models have a lower-than-passive traction of -28% .

3.2.1. Kinematics

Trench motions are almost independent of inter-plate friction (solid lines in Fig. 6a), where a range of re-normalized friction coefficients till

Table 4
Estimated valid traction range (Min. and Max.) and passive and reference traction values in $\text{N} \cdot \text{m}^{-1}$.

	Min.	Passive	Reference	Max.
DR80	$2.2 \cdot 10^{12}$	$2.2 \cdot 10^{12}$	$5.8 \cdot 10^{12}$	$1 \cdot 10^{13}$
DR60	$7.2 \cdot 10^9$	$1 \cdot 10^{12}$	$7.2 \cdot 10^{11}$	$5 \cdot 10^{12}$

about 0.2 is investigated. Over this range, plate motions are decreased by about 15% (Fig. 6b). Additionally, a maximum increase in deep slab dip of 2° is observed (Fig. 6c).

A large range of overriding plate tractions does, however, significantly influence trench motions (purple lines in Fig. 6a). When traction values are quadrupled, trench retreat rates are almost doubled. Plate motions are moderately decreased for all realistic tractions (Fig. 6b). Deep slab dip is inversely correlated with traction and is affected moderately, with differences of up to 10° for a reasonably wide range of tractions (Fig. 6c). If one increases overriding plate traction exorbitantly to $2.9 \cdot 10^{13} \text{ N} \cdot \text{m}^{-1}$, a value that results in an overriding plate absolute velocity at the upper limit of velocities observed today (Gripp and Gordon, 2002), dips as low as 23° can be reached, as shown in van Dinther (2009).

Subduction velocities and slab dip are not sensitive to about one and a half order variations in overriding plate viscosity (yellow circles in Fig. 6).

Overall, the impact of an overriding plate on slab dynamics depends heavily upon the overriding plate trench-ward motion. For a trench-ward moving overriding plate, as is assumed in the DR80-models, trench retreat rates are increased, where as slab dips are decreased

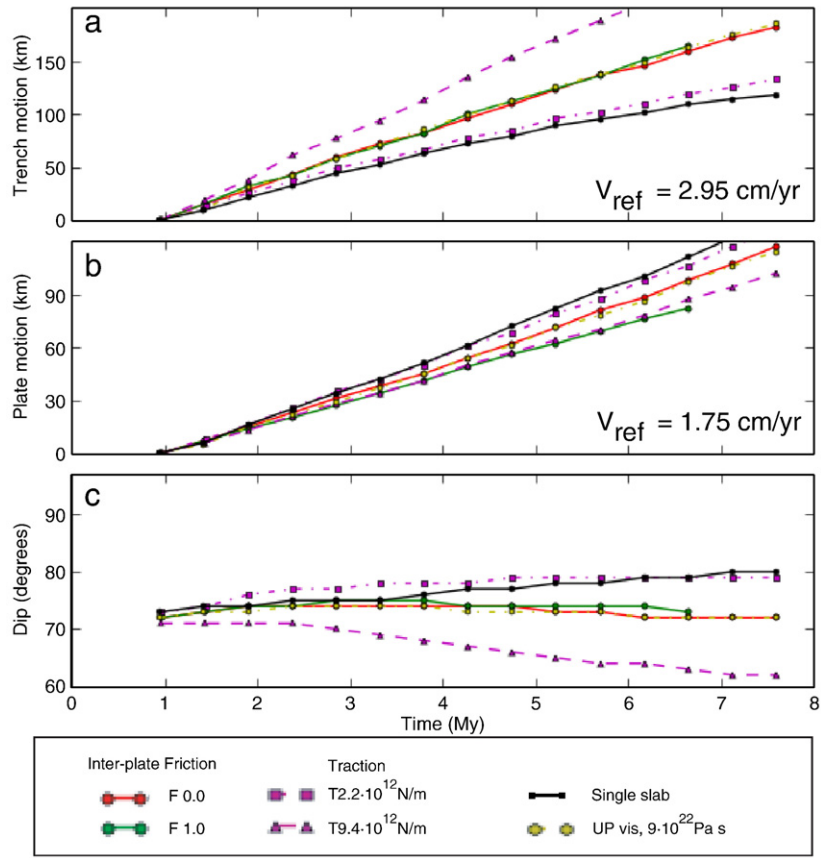


Fig. 6. (a) Amount of trench motion, (b) amount of subducting plate motion, and (c) slab dip angle evolving over time for a subducting and overriding plate configuration for a density contrast (DR) of $80 \text{ kg} \cdot \text{m}^{-3}$ and overriding plate traction (T) of $5.8 \cdot 10^{12} \text{ N} \cdot \text{m}^{-1}$. Solid colored lines indicate different inter-plate frictions. The purple lines for different overriding plate tractions. The black line represents the single slab model. The yellow dashed line with circle markers (UP vis) describes models characterized by an overriding plate viscosity of $9 \cdot 10^{22} \text{ Pa} \cdot \text{s}$ instead of $2.7 \cdot 10^{21} \text{ Pa} \cdot \text{s}$. Actual inter-plate shear stress is shown in Fig. 11. Inter-plate friction does not affect trench motions and slab dip, while overriding plate motion does so distinctly.

accordingly. An overriding plate cannot seemingly decrease trench retreat for distinctly retreating trenches (Fig. 6a,c). Independent of overriding plate traction, the addition of an overriding plate results in a decrease of plate motion (Fig. 6b).

3.2.2. Topography

The subduction zone morphology is analyzed using trench profiles in Fig. 7. Decreasing slab pull results in an increase in shallow dip (0–100 km) (Fig. 7a,b), which is also observed in a single slab

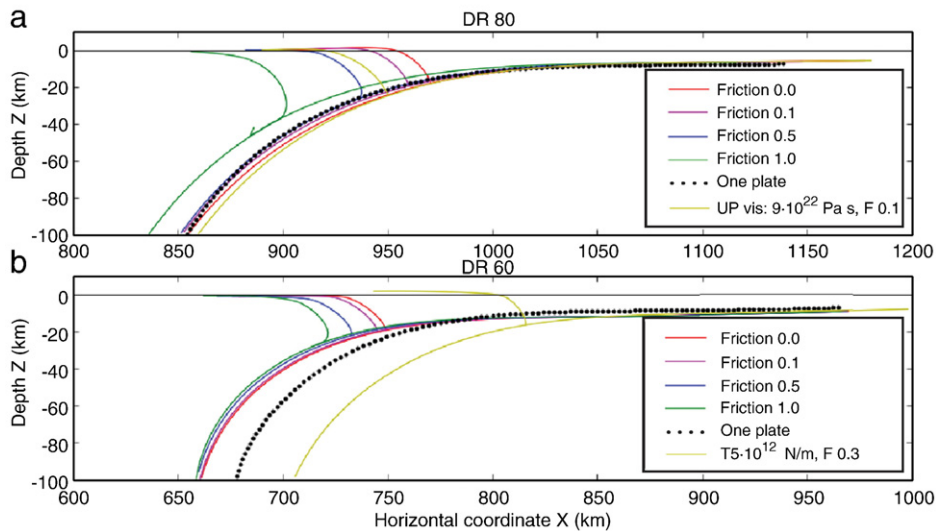


Fig. 7. Trench topography for different inter-plate frictions (solid colored lines) at $t_{TP} = 6.65$ My for a density contrast of (a) $80 \text{ kg} \cdot \text{m}^{-3}$, and (b) $60 \text{ kg} \cdot \text{m}^{-3}$. Topography of a single subducting plate is shown as a dotted black line. The yellow line represents an overriding plate with a higher viscosity ($9 \cdot 10^{22} \text{ Pa} \cdot \text{s}$) and high overriding plate traction ($5 \cdot 10^{12} \text{ N} \cdot \text{m}^{-1}$) in panel a and b, respectively. Actual inter-plate shear stress is shown in Fig. 11. Increasing inter-plate friction increasingly drags the overriding plate down.

configuration. An increase in inter-plate friction results in an overriding plate that is increasingly dragged down along the subducting plate leading to a deeper plate intersection, where vertical differences are as great as 20 km. It is interesting to observe that increasing friction to 0.5 and above leads to the formation of a local inward triangular corner just above the trench (Fig. 7a,b).

As a result of an increasing overriding plate trench-ward motion, the overriding plate over-thrusts the slab further, thereby decreasing trench depth significantly (Fig. 7b). It also slightly decreases shallow dip, so a larger radius of curvature is observed for faster trench-ward overriding plate motions.

Increasing overriding plate viscosity by about one and a half order, thereby making it stronger, results in a slightly smaller radius of curvature (Fig. 7a). Additionally, a decrease in backstop dip for stronger overriding plates is observed.

The addition of an overriding plate results in a minor, though consistent decrease in shallow slab dip (Fig. 7a,b).

A more detailed look at the height of the overriding plate bulge shows it is inversely correlated with inter-plate friction (Fig. 8). Inter-plate friction influences bulge height and presence significantly, showing a variation from 0.67 km below sea level to about 1.63 km above sea level. The presence of an overriding plate bulge depends, however, mainly on sufficient overriding plate trench-ward motion, as is evident from the large difference between DR80 and DR60-model sets. Overriding plate trench-ward motion should be larger than $0.035 \text{ cm}\cdot\text{yr}^{-1}$. Another factor that influences the elevation of the overriding plate bulge is overriding plate strength (yellow dot, Fig. 8). Increasing overriding plate viscosity by one order reduces overriding plate topography by about 0.47 km or 35% to 0.87 km above sea level.

3.2.3. Stresses

Stresses originating from slab bending are slightly inversely correlated with inter-plate friction (-0.19 for DR80, less for DR60 from Fig. 9a). Faster trench-ward overriding plate motions result in

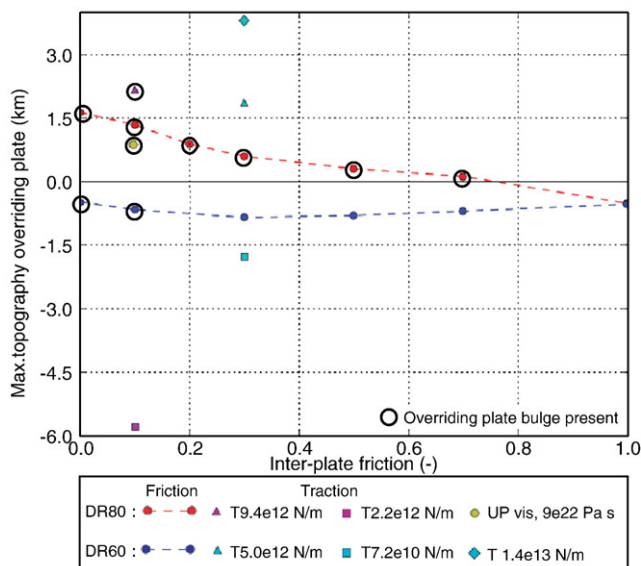


Fig. 8. Maximum topography of the overriding plate bulge, relative to imposed geoid or sea level, as a function of inter-plate friction for density contrasts of 80 (red dots) and 60 (blue dots) $\text{kg}\cdot\text{m}^{-3}$, different overriding plate tractions (purple and cyan dots resp.), and increased overriding plate viscosity (yellow dot). Maximum height is measured within 60 km from trench at $t_{TP}=6.65$ My. Note that the peculiar deep location of DR80 with a traction of $2.2\cdot 10^{12} \text{ N}\cdot\text{m}^{-1}$ results from overriding plate detachment from the subducting lithosphere. Actual inter-plate shear stress is shown in Fig. 11. If overriding plate trench-ward motion is pertinent, inter-plate friction demotes overriding plate topography.

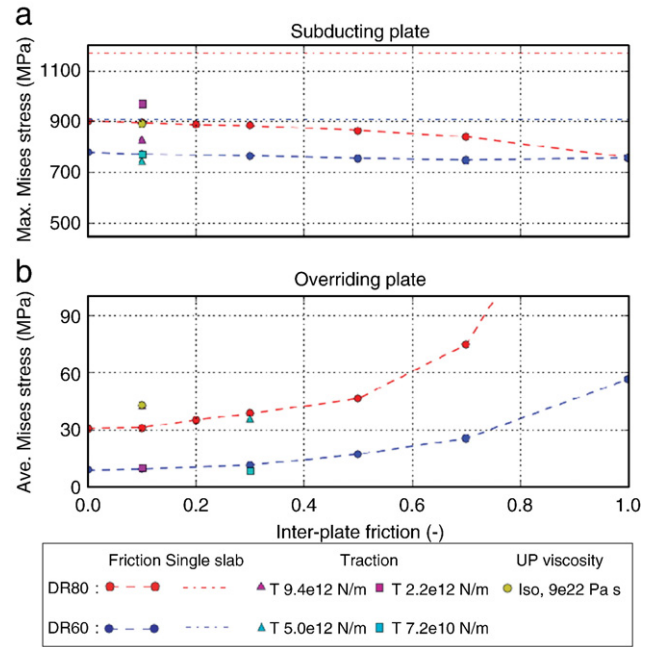


Fig. 9. Two types of measurements of Mises stress (MPa) for a two plate configuration; (a) maximum Mises stress in the slab, which is an extensional stress within the shallow bending region, and (b) average Mises stress in the overriding plate within 7 km of the inter-plate fault. Shapes show different density contrasts of 80 (red dots) and 60 (blue dots) $\text{kg}\cdot\text{m}^{-3}$, different overriding plate tractions (purple and cyan dots resp.), and increased overriding plate viscosity (yellow dot). Time is $t_{TP}=6.65$ My. Note that maximum Mises stress occurs only over a limited area within the top stretching region of the stronger core and decreases markedly further away. Actual inter-plate shear stress is shown in Fig. 11.

lower maximum bending stresses in the slab and higher stresses in the overriding plate (blue and purple dots, Fig. 9a and b resp.). Stress build-up in the overriding plate strongly depends on the overriding plate rheology (yellow dot, Fig. 9b), i.e., one order of magnitude increase in overriding plate viscosity results in a stresses increase of 38%. Overall, including an overriding plate leads to a slight shallow unbending of the slab and an accompanying decrease in slab bending stresses of about 30% for DR80 and 15% for DR60 (Fig. 9a).

3.2.4. Frictional dissipation

Frictional dissipation generally increases over time, and a steady-state increase occurs for inter-plate frictions of 0.5 and lower and a non-linear departure occurs for an inter-plate friction of 1.0 (Fig. 10). The explosive and unstable departure of this friction indicates that a limit for stable subduction has been reached. Frictional dissipation correlates with both inter-plate friction, which is the dominant factor, and overriding plate traction.

4. Discussion

4.1. Single subducting plate

To understand the role of an additional overriding plate, it is necessary to first define the main controlling mechanisms of slab dynamics in a single plate setup. The role of slab buoyancy is highly important (e.g., Forsyth and Uyeda, 1975), but has been extensively investigated (e.g., Vlaar and Wortel, 1976; Chapple and Tullis, 1977; Conrad and Lithgow-Bertelloni, 2002; Schellart, 2004b), so that the focus is aimed at the role of; a) mantle flow pressure within the oceanic corner, varying through changes in slab width and other non-induced mantle flow sources, b) slab–mantle viscosity contrast, and c) ridge push.

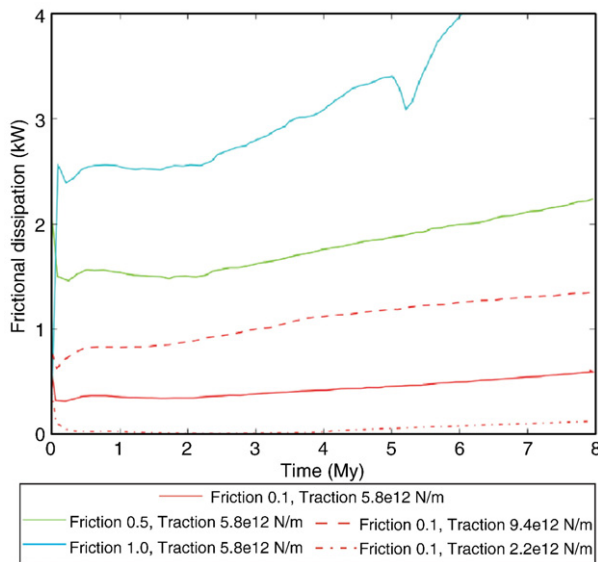


Fig. 10. Frictional dissipation along the inter-plate fault through time, which increases for both increasing inter-plate frictions (colored solid lines) and for increasing overriding plate tractions (red line with different styles) and increases over time. The jump for a friction of 1.0 is a model-related disruption event as can be seen in Fig. 7. Actual inter-plate shear stress is shown in Fig. 11.

4.1.1. Role of local mantle flow pressure

Larger trench-parallel slab widths and additive mantle flow increase flow pressure in the oceanic corner below the slab. The former increases flow pressures through an increase in work required for mantle flow to circulate toroidally around the slab. The increased flow pressure directly beneath the trench opposes trench retreat, ultimately causing trench retreat to cease completely (Fig. 3a). Trench advance is caused by continuous plate movement that is driven by ridge push. A slower trench retreat for increased slab width is in general agreement with analogue (Funicello et al., 2006), hydrodynamic (Dvorkin et al., 1993), and numerical models (Stegman et al., 2006; Royden and Husson, 2006; Piromallo et al., 2006; di Giuseppe et al., 2008; Honda, 2008). Furthermore, an extensive study of world-wide trench migration velocities showed that slab width is likely a dominant factor in determining trench retreat rates (Schellart et al., 2008).

4.1.2. Role of viscosity contrast

Increasing the viscosity contrast between the slab and surrounding mantle leads to a significant decrease in slab dip and a significant increase in trench and plate velocities (Fig. 4). This is in accordance with Capitanio et al., (2007), who explain this relationship by assuming that the strength of the slab determines slab geometry and that moving a slab laterally through a less viscous mantle is favored, energetically, over bending a highly viscous slab. Stronger slabs that produce more roll back are also observed in free subduction analogue (Bellahsen et al., 2005; Funicello et al., 2008) and numerical models (Funicello et al., 2003a; Capitanio et al., 2007; Goes et al., 2008).

However, the opposite result is predicted by Conrad and Hager (1999). From a predefined slab and fault configuration, they predict a velocity decrease because resistance to bending increases with slab strength. This reversed behavior is, moreover, observed in numerical results with a viscous or visco-plastic slab rheology, where maximum stresses near the trench cause the slab to yield. Consequently, plate strength is locally dissolved and slab steepening is facilitated (Becker et al., 1999; Enns et al., 2005; Stegman et al., 2006). This explanation has been put forth in order to explain the apparent paradox that the oldest and, therefore, strongest subducting plates in the world, located in the western Pacific, often dip vertically (di Giuseppe et al., 2009).

4.1.3. Role of ridge push

Stress propagation through the plate is guaranteed by a strong, high viscosity core. The effect of a dynamic ridge push on the subducting lithosphere is, however, almost negligible in terms of trench velocities and slab dip (Fig. 3). These results agree with general estimates of ridge push that consider it to be about one order of magnitude less than slab pull (e.g., Kearey and Vine, 1996). A possible, though not investigated, factor that could increase the influence of ridge push distinctly is a low viscosity asthenosphere (Capitanio et al., 2007).

4.1.4. Comparison to observations

Based on a comparison with kinematic and geometric observations, a 20 km foundation with a density contrast of $80 \text{ kg} \cdot \text{m}^{-3}$ is selected as a reference model. This model shows trench velocities within the observed range of either 1 and $5 \text{ cm} \cdot \text{yr}^{-1}$ (Garfunkel et al., 1986), -5 to $5 \text{ cm} \cdot \text{yr}^{-1}$ (Heuret and Lallemand, 2005), or -8 to $12 \text{ cm} \cdot \text{yr}^{-1}$ (Gripp and Gordon, 2002), where different estimates depend on the frame of reference (Schellart, 2008). Observed subduction velocities range mainly between 4 and $9 \text{ cm} \cdot \text{yr}^{-1}$ (Jarrard, 1986; Conrad and Hager, 1999; Lallemand et al., 2005; Heuret et al., 2007), where these parameters lead to a subduction velocity of about $5 \text{ cm} \cdot \text{yr}^{-1}$. This is accompanied by a slab dip of about 70° , which is close to the average of 65° – 70° (Jarrard, 1986).

In conclusion, our single slab model is overall consistent with well-accepted modeling results and observations.

4.2. Subducting and overriding plates

To assess the role of an overriding plate and the characteristics of the interaction between the subducting and overriding plates, the two most interesting parameters are analyzed, a) inter-plate friction, and b) overriding plate traction.

4.2.1. Role of inter-plate friction

Observed frictional effects must be interpreted taking into account that the model pressures on the fault are not realistic due to an underestimation of lithostatic pressures that results from the Archimedes body force. Given that shear stress is proportional to the normal pressure on the fault, friction values do not correspond to the real friction values, and must be renormalized by the ratio of real over modeled pressures.

The investigated friction coefficients from 0.0 to 1.0, after renormalization, correspond to real values in the order of 0.02 to 0.2. This range encompasses the interesting friction range that is apparent in numerous other subduction models that require a friction coefficient of $O(0.1)$ for continuous subduction (Zhong and Gurnis, 1994; Zhong et al., 1998) and for reproduction of subduction observables (Hassani et al., 1997; Buiter et al., 2001; Sobolev and Babeyko, 2005; de Franco et al., 2007). For a proper comparison to literature, applied friction values are converted to the actual shear stress measured at the fault. The resisting tangential stress τ is averaged over time (1–5 My) and depth along the fault and is plotted in Fig. 11 for each model.

Estimates of the strength that a subduction fault can support range from a lower bound of 3–30 MPa (resp. Toth and Gurnis, 1998; Molnar and England, 1990) to an upper bound of 20–100 MPa (resp. Hickman, 1991; Hanks, 1977). The free-moving trench models presented in this study show that even an applied shear stress of 58 MPa results in continuous subduction (Fig. 6a). Although, shear stresses larger than about 35 MPa trigger extreme overriding plate stresses (Fig. 9b), trench topographies (Fig. 7a) and unstable fault behavior (Fig. 10). These values, however, need to be interpreted cautiously because, in order to draw fully reliable conclusions, models with realistic pressures throughout the plates should be run.

Frictional resistance opposes subduction by a decrease in plate motions, while trench motions remain unaffected for frictions within

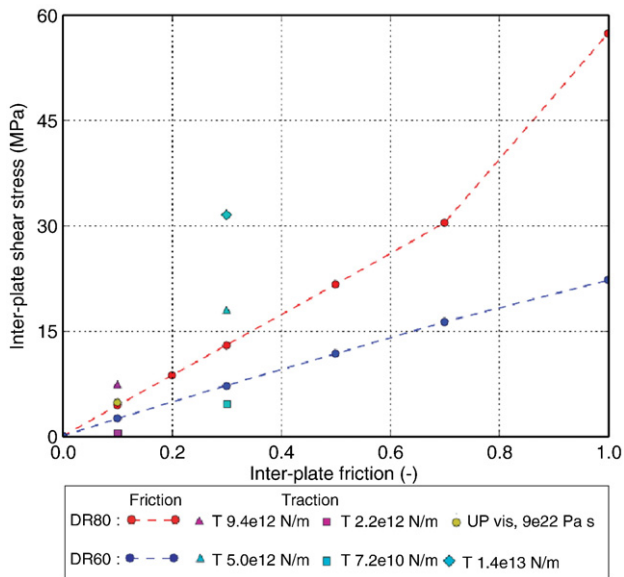


Fig. 11. Average measured shear stress τ_{crit} at the inter-plate fault versus inter-plate friction μ . The resisting tangential stress τ is calculated at each overriding plate node that lines up with the inter-plate fault, using $\tau_{crit} = \mu\sigma_n$. The normal pressure σ_n is calculated using stress values and local dip orientations from our models. Shear stresses are averaged over time (1–5 My) and depth along the fault. Shapes show different density contrasts of 80 (red dots) and 60 (blue dots) $\text{kg}\cdot\text{m}^{-3}$, different overriding plate tractions (purple and cyan dots resp.), and increased overriding plate viscosity (yellow dot). Note that the difference between DR80 and DR60 is caused by different relative overriding plate tractions.

our limited range till about 0.2. A significant impact of frictional resistance is, however, observed for local overriding plate topography and stresses.

Increased inter-plate coupling increasingly drags the overriding plate down with the slab, thereby deepening the trench and inhibiting the growth of a positive overriding plate topography (Fig. 7). The qualitative inversely proportional relationship between inter-plate friction and overriding plate topography is in accordance with the numerical models of [Tharp \(1985\)](#), [Whittaker et al. \(1992\)](#), [Hassani et al. \(1997\)](#), [Cattin and Lyon-Caen \(1997\)](#), [Buitter et al. \(2001\)](#), [Hampel and Pfiffner \(2006\)](#), [Krien and Fleitout \(2008\)](#).

The local inward-corner within the overriding plate, formed for frictions of 0.5 or larger (Fig. 7), acts as a channel entrance for the entrainment, or down-dragging, of potential wedge material. Inter-plate frictions, therefore, play a key role in distinguishing wedge behavior. High inter-plate frictions promote subduction erosion over wedge isolation and accompanying exhumation, as demonstrated in [van Dinther \(2009\)](#).

Increased inter-plate coupling, moreover, leads to a larger radius of curvature and overall shallower slab (Fig. 7), since coupling helps to unbend the slab, as seen in [Billen and Hirth \(2007\)](#). This slightly reduces bending stresses within the slab, although the influence is only distinct if the plate coupling is induced by a distinctly advancing overriding plate (Fig. 9). The minor influence of frictional resistance on bending stress ($\sim 10\%$) suggests that subducting plate stresses are mainly the result of bending resistance, which agrees with the results of [Conrad and Hager \(1999\)](#). The slightly deeper slab for lower frictions can also result from an increase in loading due to overriding plate topography, which exerts an additional normal stress on the system. The distinction and discussion of this loading is, however, beyond the scope of this paper.

Frictional dissipation is observed to increase over time (Fig. 10). This is most likely the result of the imposed overriding plate traction, which corresponds to an actively advancing overriding plate. This causes thickening, as observed by [Heuret et al. \(2007\)](#), which means an increase in both the length of the fault l_f (+21% in 8 My for the reference model) and the lithostatic pressures and corresponding

normal pressures on the plate contact. Both of these effects increase total shear stress τ_f at the fault and thereby the energy Φ_f^{vd} dissipated on it, as formulated in the viscous fault dissipation formulation by [Conrad and Hager \(1999\)](#):

$$\Phi_f^{vd} = \tau_f v_p l_f \quad (1)$$

In this formulation, which is also a reasonable approximation of dissipation on brittle faults because these also support shear stresses to some degree, v_p is best approximated by subduction velocity v_{sub} . The observed increase in frictional dissipation with trench-ward overriding plate motion and friction are explained by a positive effect on shear stress τ in Eq. (1). The former parameter acts through a direct increase in normal pressures on the fault, which is again amplified by an increase in fault length and lithostatic pressures.

4.2.2. Role of overriding plate motion

An increase in trench-ward overriding plate movement increases trench retreat significantly (Fig. 6a), as it acts as an indenter that forces a retreat. Elevating overriding plate motion eventually forces a transition from slab-driven trench migration, primarily driven by slab buoyancy, to overriding-plate driven trench migration, primarily resulting from the lateral motion of the overriding plate (Fig. 6), as defined by [Heuret et al. \(2007\)](#) and [Schellart \(2008\)](#). The indentation also adds upward momentum that actively decreases slab dip (Fig. 6c). The association of shallow dipping slabs with advancing overriding plates is confirmed by a statistical analysis of observations by [Jarrard \(1986\)](#) and [Lallemand et al. \(2005\)](#) and is first suggested by [Cross and Pilger \(1978\)](#) and [Vlaar \(1983\)](#). The observation is also consistent with analogue ([Heuret et al., 2007](#)) and numerical models ([Christensen, 1996](#); [Olbertz et al., 1997](#)).

Additionally, results, which are not presented here, show that if trench motion is already less than a few millimeters per year, an overriding plate traction lower than passive slows a single slab down and can even cause trench advance ([van Dinther, 2009](#)). This is due to hydrostatic suction, which draws the slab forward and upward to prevent separation of the plates ([Bott et al., 1989](#); [Whittaker et al., 1992](#); [Chemenda, 1993](#)). This coupling was already suggested by [Carlson and Melia \(1984\)](#) in order to explain the Izu–Bonin–Mariana trench advance. The decrease in trench motion allows more time for slab bending and increases deep slab dip (Fig. 6c), although shallow slab dip is decreased (Fig. 7a,b). This overriding plate motion-deep slab dip relationship agrees with the findings of [Heuret et al. \(2007\)](#).

An overriding plate trench-ward velocity of about $8 \text{ cm}\cdot\text{yr}^{-1}$, leads to shallow, though not flat plateau, subduction ([van Hunen, 2001](#)) with slab dips up to 23° . Trench-ward overriding plate motion is one of the possible explanations for shallow slabs ([van Hunen et al., 2004](#)), which is particularly interesting for parts of the Andes, as South America is actively moving trench-ward at velocities of $2\text{--}3 \text{ cm}\cdot\text{yr}^{-1}$ (e.g., [Chase, 1978](#); [Gordon and Jurdy, 1986](#); [Silver et al., 1998](#); [van Hunen et al., 2002b, 2004](#)). The occurrence of flat plateau subduction, would at least require an additional, forced subduction of large buoyant ridges or plateaus, as suggested by [Gutscher et al. \(2000\)](#); [van Hunen et al., 2002a,b](#); [Espurt et al. \(2008\)](#).

Trench-ward overriding plate motion was seen to be an influential and necessary component for overriding plate topography (Fig. 8). An increase in trench-ward motion causes the overriding plate to thrust up more over the slab and thereby create an overriding plate bulge, located above the shallowest part of the slab. Additionally, the accompanying increase in horizontal compression is necessary to propel the overriding plate upward, amplifying the relative topography of the bulge. The key role of trench-ward overriding plate motion in the development of overriding plate topography is consistent with results from [Hampel and Pfiffner \(2006\)](#). [Buitter et al. \(2001\)](#) also observed an increase in overriding plate topography for absolute trench-ward moving overriding plates.

4.2.3. Role of an overriding plate

The acquired understanding of the role of inter-plate friction and overriding plate motion provides a background to assess the impact of an overriding plate on slab dynamics. The inclusion of an overriding plate added three forces to the single slab system; frictional resistance (resists slab forward motion), indentation (pushes the slab in retreat), and hydrostatic suction (acts to prevent separation).

Frictional resistance only slightly influences shallow slab parameters, such as shallow slab dip, corresponding bending stresses, and plate motion (Figs. 7, 9, and 6 resp.). However, it strongly affects local overriding plate geometry and stresses (Fig. 5). This suggests a frail contact zone and direct surroundings that is bounded by a robust subduction system. In this system, indentation is highly important, if there is an indication for a distinct trench-ward moving overriding plate. The role of hydrostatic suction is minor, as it is only influential if trenches are near-stationary, although the radius of the curvature is slightly increased in general. The minor role of hydrostatic suction is in accordance with the results of Pacanovsky et al. (1999), who estimated numerically that trench suction forces can reach no more than 10% of slab pull forces. Overall, the role and impact of the overriding plate is fully determined by overriding plate movement and tectonic conditions within the overriding plate. Therefore, if trench-ward overriding plate motion is negligent, the modeling of a single slab sinking in a mantle is a reasonable approximation for understanding large-scale slab dynamics.

In this study, an obviously simplified model was used to acquire a first impression of lithospheric interaction at convergent margins. We realize that a simple Coulomb frictional formulation in a lithostatic pressure underestimated framework is not able to grasp the full complexity of plate coupling, and a more realistic formulation will be the subject of further studies. Moreover, it would be reasonable to adopt a more dynamic formulation for overriding plate traction, although this approach did allow for a broad assessment of the role of overriding plate motion for all possible forces. Finally, it is noted that the influence of frictional resistance and overriding plate presence might be underestimated due to a small overriding plate thickness, which is representative of an oceanic lithosphere in a hot island arc region (Kelemen et al., 2003).

5. Conclusions

This study addressed the impact and role of an overriding plate and inter-plate fault characteristics on slab and overriding plate dynamics in a buoyancy-driven subduction framework.

A single slab interacting with a mantle showed that distinct variations in local mantle flow pressure can influence slab dynamics considerably. Wider slabs and additional local mantle flow sources increase flow pressures directly below the trench, thereby effectively repressing trench retreat, increasing slab dip accordingly, and can ultimately even lead to trench advance. For high viscosity slabs, energetically expensive bending energy is minimized, resulting in more roll back.

In a subducting and overriding plate configuration, frictional resistance, for friction coefficients ranging up to about 0.2 or shear stresses over a range of ~0–58 MPa, has little regional to global effect on slab dynamics, as trench motions and deep slab dip are almost unaffected. Locally, effects are more pronounced as frictional resistance strongly affects local overriding plate topography and stresses. Increased coupling drags the overriding plate down, thereby inhibiting topographic growth on the overriding plate. Furthermore, plate motions can be decreased by about 15% and slab bending stresses by about 10%.

The role of trench-ward overriding plate motion on slab dynamics is more important, as additional indentation enforces a sharp trench retreat and decrease in slab dip. Trench-ward overriding plate motion is also required for the presence of overriding plate mountain building.

Overall, the impact of an overriding plate on trench motions and deep slab dip is fully determined by overriding plate motion and the

tectonic conditions within the overriding plate. Overriding plate influence is only pertinent if the overriding plate actively advances the trench.

Acknowledgements

We thank Rinus Wortel and Rob Govers for their comments on an initial draft of this manuscript. The manuscript also benefited from the reviews of Leigh Royden and an anonymous reviewer. We also would like to thank Giacomo Corti, Giorgio Ranalli and Dimitrios Soukotas as the editors of this special volume. This research has been supported by the EURYI (European Young Investigators) Awards Scheme (Eurohorcs/ESF, responsible F.F.) with funds from the National Research Council of Italy and other National Funding Agencies participating in the 3rd Memorandum of Understanding, as well as from the EC Sixth Framework Program. It, moreover, received financial support from the Prestige Master Programme 'System Earth Modeling' of Utrecht University. Computations were conducted at the Institute of Geophysics at ETH Zurich.

Appendix A. Subducting plate

The downgoing plate is 1800 km long and 70 km thick (Fig. 1 and Table 1) and represented by a Lagrangian grid of 33×10 first-order bilinear plane strain continuum elements.

A constant slab-upper mantle density contrast varying from $40 \text{ kg} \cdot \text{m}^{-3}$ to $80 \text{ kg} \cdot \text{m}^{-3}$ is applied. Hereby important variations in density, resulting from thermal conduction and phase transitions, are neglected as subduction occurs at a significantly faster rate than conduction ($v_{\text{sub}} > 1 \text{ cm} \cdot \text{yr}^{-1}$; Peclet number $\gg 1$; Turcotte and Schubert, 2002). A second driving force, generally believed to be of a second order of importance (Forsyth and Uyeda, 1975), is a horizontal ridge push force that is applied as a constant distributed load of $3 \cdot 10^{12} \text{ N} \cdot \text{m}^{-1}$ at the trailing end. This force is representative of an oceanic lithosphere of 80 My as integrated over plate-buoyancy gradients (Turcotte and Schubert, 2002) and is within the estimated range of Parsons and Richter (1980). At the free trailing end, a vertical mirror boundary condition is applied to mimic horizontal pressures resulting from a horizontally extended plate. A constant linear temperature profile from $T_0 = 0 \text{ }^\circ\text{C}$ to $T_{\text{LAB}} = 1300 \text{ }^\circ\text{C}$ is assumed in order to determine the viscosity profile and rheological strength of the subducting lithosphere.

The rheology of the subducting plate is that of a layered linear Maxwell viscoelastic body. Fixed values of 200 GPa and 0.3 for respectively bulk Young's modulus E and Poisson's ratio ν are used after Capitanio et al. (2007), granted that a large variation of elastic moduli does not influence large-scale slab motions or stress values. Viscous behavior is defined by a linear time-independent power law. A layered viscosity profile with a strong core (Fig. 1, Inset B) simulates strength profiles that are the natural result of a slab's thermal gradient and, thereby, mimics a temperature-dependent rheology (Morra and Regenauer-Lieb, 2006a; Capitanio et al., 2007). A reference viscosity profile with an average viscosity of $6.5 \cdot 10^{23} \text{ Pa} \cdot \text{s}$ (Lay23) is used. This results in a slab-upper mantle viscosity contrast of around two and a half orders, as is deemed generally reasonable (Zhong and Gurnis, 1995a; Billen et al., 2003).

Appendix B. Overriding plate

The overriding plate is a 230 km long and 40 km thick young oceanic lithosphere (Fig. 1 and Table 1). It is made up of 100×16 first-order bilinear plane-strain continuum elements.

An initial configuration with two adjacent tectonic plates is created (Fig. 5a,b), which is subsequently allowed to adapt freely to the systems dynamics. Lateral continuity during the systems evolution is ensured by a horizontal bottom traction, representing:

a) induced arc corner flow, b) ridge push from the overriding oceanic plate, and c) a possible, additional far-field push. To accommodate this large range of possible forces, a wide range of traction values is investigated ($7.2 \cdot 10^9$ – $2.9 \cdot 10^{13} \text{ N} \cdot \text{m}^{-1}$). The magnitude of this traction determines whether the overriding plate either passively follows a retreating slab or enforces trench retreat or advance. Acceptable magnitudes for ridge push integrated over thickness are 10^{12} – $10^{13} \text{ N} \cdot \text{m}^{-1}$ for about 100 My-old plates (Turcotte and Schubert, 2002), while much smaller values are acceptable for younger oceanic lithospheres. Additionally, induced arc corner flow pressures below the overriding lithosphere are in the order of 10^{13} N/m (Turcotte and Schubert, 2002). Finally, as in a subducting plate, the trailing end of the overriding plate has a mirror boundary condition to mimic its extension. The density of the visco-elastic overriding plate is similar to that of the subducting plate (Table 1), while its viscosity profile differs as a stronger core has not yet developed and a 7 km oceanic crust is included (Fig. 1, Inset B).

Appendix C. Lithosphere–mantle interaction

Subducting and overriding plates are supported and affected by a horizontally unbounded upper mantle, whose contribution is expressed by: a) a set of dissipative drag forces, b) an Archimedes compensating upward body force, c) an isostatic restoring force, and d) an additional mantle flow component. The upper mantle is confined by a 10% density increase representing the 660 km-discontinuity.

a) A solid lithosphere that descends with velocity U in a viscous fluid is subjected to a drag force F_{drag} , $F_{\text{drag}}^- = \bar{K} \cdot \bar{U}$, which is applied to the lithosphere through a set of horizontal and vertical dissipative dash-pots located at the green line in Fig. 1. As in Capitanio et al. (2007), the drag coefficients K_x and K_z depend on mantle viscosity and are analytically calculated by assuming a $1000 \times 1000 \text{ km}^2$ (LxWi) plate, extending to the 660-km discontinuity at a dip of 65° . This setup captures the dynamic and energetic 3-D response of a solid object descending in a Stokes fluid as described and benchmarked in Morra (2004).

b) Both lithospheres are subjected to an Archimedes upward body force, $Ar = \rho_M \cdot g$ ($\text{N} \cdot \text{m}^{-2}$ in 2-D), to compensate for the displacement of mantle material up to a predefined equipotential surface, which is approximately the Earth's sea level (Geoid, as in Fig. 1). In previous models (Funicello et al., 2003a; Morra and Regenauer-Lieb, 2006a; Morra and Regenauer-Lieb, 2006b; Capitanio et al., 2007) this component was implemented as a pressure, applied to the bottom and integrated over lithosphere thickness h , $\rho_{\text{Mantle}} \cdot g \cdot h$.

c) When negative topography is created on the bottom of both lithospheres, specifically near the trench, mantle material is displaced, resulting in a pressure deficit on that location. This deficit causes an isostatic response in the form of an upward non-dissipative elastic force, $P_{\text{Wi}} = (\rho_M - \rho_W) \cdot g \cdot z$, which is linearly proportional to the amount of deflection z . This pressure ($\text{N} \cdot \text{m}^{-1}$ in 2-D) is applied at the bottom of both lithospheres and serves as a Winkler foundation P_{Wi} (Winkler, 1867; Hetenyi, 1946). In reality, the pressure at the bottom of the lithosphere results from the mantle flow pressures present. A 2-D analytical solution for induced flow pressure is available by solving a force balance between pressure, gravity and viscous forces for a simplified geometry (Turcotte and Schubert, 2002). The slab induced flow pressure, relative to hydrostatic pressure, can be separated into two components; $P_{\text{Oceaniccorner}}$, along the bottom of the slab, and $P_{\text{Arccorner}}$, in the mantle wedge or arc corner, along the top of the slab (Dvorkin et al., 1993):

$$P_{\text{Oceaniccorner}} = \frac{0.462\eta v_{\text{sub}}}{r} \quad (2)$$

$$P_{\text{Arccorner}} = \frac{-8.558\eta v_{\text{sub}}}{r} \quad (3)$$

In these equations, r is distance along the bottom of the descending slab, assuming a slab dip of 45° . The solution in Fig. 12 (resp. blue and purple line) is found by assuming a subduction velocity v_{sub} of 5 cm/yr, the average steady-state subduction velocity of the reference model. In this model, both flow pressures are applied along the bottom of the slab and, together, result in a total induced flow pressure depicted by the green line in Fig. 12. The total induced flow pressure intersects the applied foundation (red line) at a depth of about 20 km, which is the approximate reference depth extent W of the foundation. This reference depth extent is confirmed in an analysis of kinematic and geometric characteristics (Section 4.1.4).

d) To account for variations in mantle flow pressure, the depth extent of the above foundation is varied extensively from 10 to 30 km. Variations in oceanic corner flow pressure can result from induced corner flow by a descending slab with variable, trench-parallel slab width and/or other external mantle flow sources, both on a global (Richard et al., 1991) and on a local scale (Russo and Silver, 1994). In case of varying slab width, flow pressure increases for increasingly wider slabs or larger trench lengths, as it requires more work for mantle material to flow sideways around the slab, as observed by e.g., Bellahsen et al. (2005), Stegman et al. (2006), Morra and Regenauer-Lieb (2006b), and Schellart et al. (2007).

Appendix D. Inter-plate fault characterization

The inter-plate contact is defined by a basic configuration of a single brittle fault plane on which the fault strength is governed by an isotropic Coulomb frictional law, $\tau_{\text{crit}} = \mu \sigma_n$, where τ_{crit} is the critical shear stress, μ is the frictional sliding coefficient and σ_n is the normal pressure at the contact. Cohesion is not involved here because sliding occurs on a pre-existing surface. Once the yield stress criterion in the Coulomb friction law is met, sliding occurs over a surface-to-surface discretized contact. A finite-sliding contact formulation is used to allow for any arbitrary separation, sliding or rotation on the fault surface. To increase the smoothness and numerical stability of the brittle contact, two numerical functions have been incorporated. First, the subducting plate is defined as the master surface to ensure that nodes of the overriding plate do not penetrate into the downgoing slab. Second, an exponential pressure-over-closure relationship is applied to prevent frequent penetration of

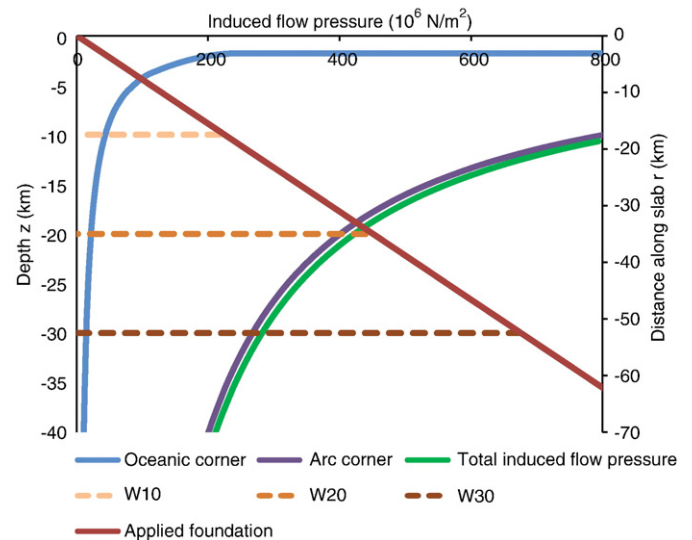


Fig. 12. Slab induced flow pressure, analytically calculated according to Turcotte and Schubert (2002). The dark red line is the applied foundation, $(\rho_M - \rho_W) \cdot g \cdot z$. Dashed lines show investigated depth extents of the foundation W of 10, 20 and 30 km. The left vertical axis shows normal depth z below the bottom of the slab and the right vertical axis shows r , distance along a 45° dipping slab.

nodes and thereby define a robust softened contact. The mutual penetration of nodes is permanently excluded by the transmission of an enormous pressure, which increases exponentially to a maximum value of 4 GPa, once the two surfaces are within an over-closure clearance distance of 250 m of each other. These functions are vital for numerical performance, but do not influence the magnitude of the resulting motions and still allow for proper transmission of shear stresses and viscous pressures.

References

- Babeyko, A., Sobolev, S.V., 2008. High-resolution numerical modeling of stress distribution in visco-elasto-plastic subducting slabs. *Lithos* 103 (1–2), 205–216.
- Becker, T.W., Faccenna, C., 2009. A review of the role of subduction dynamics for regional and global plate motions. In: Lallemand, S., Fuciniello, F. (Eds.), *International Journal of Earth Sciences. Special Volume: Subduction Zone Geodynamics*. Springer-Verlag, Berlin, p. 33.
- Becker, T., Faccenna, C., O'Connell, R.J., 1999. The development of slabs in the upper mantle: insights from numerical and laboratory experiments. *J. Geophys. Res.* 104 (B7), 15207–15226.
- Bellahsen, N., Faccenna, C., Fuciniello, F., 2005. Dynamics of subduction and plate motion in laboratory experiments: insights into the plate tectonics behavior of the earth. *J. Geophys. Res.* 110, 1–15.
- Billen, M.L., 2008. Modeling the dynamics of subducting slabs. *Annu. Rev. Earth Planet. Sci.* 36, 325–356.
- Billen, M., Hirth, G., 2007. Rheologic controls on slab dynamics. *Geochem. Geophys. Geosyst.* 8 (Q08012), 24.
- Billen, M., Gurnis, M., Simons, M., 2003. Multiscale dynamic models of the Tonga-Kermadec subduction zone. *Geophys. J. Int.* 153, 359–388.
- Bott, M., Waghorn, G., Whittaker, A., 1989. Plate boundary forces at subduction zones and trench-arc compression. *Tectonophysics* 170, 1–15.
- Buffet, B., Rowley, D., 2006. Plate bending at subduction zones: consequences for the direction of plate motions. *Earth Planet. Sci. Lett.* 245, 359–364.
- Buiter, S.J., Govers, R., Wortel, M.R., 2001. A modelling study of vertical surface displacements at convergent plate margins. *Geophys. J. Int.* 147, 415–427.
- Capitanio, F., Goes, S., Morra, G., 2007. Dynamic models of downgoing plate-buoyancy driven subduction: subduction motions and energy dissipation. *Earth Planet. Sci. Lett.* 262, 284–297.
- Carlson, R., Melia, P., 1984. Subduction hinge migration. *Tectonophysics* 102, 1–16.
- Cattin, R., Lyon-Caen, H., 1997. Quantification of interplate coupling in subduction zones and forearc topography. *Geophys. Res. Lett.* 24 (13), 1563–1566.
- Chapple, W., Tullis, T., 1977. Evaluation of forces that drive plates. *J. Geophys. Res.* 82, 1967–1984.
- Chase, C., 1978. Extension behind island arcs and motions relative to hot spots. *J. Geophys. Res.* 83, 6729–6749.
- Chemenda, A., 1993. Subduction of lithosphere and back-arc dynamics: insights from physical modelling. *J. Geophys. Res.* 99, 16167–16185.
- Christensen, U., 1996. The influence of trench migration on slab penetration into the lower mantle. *Earth Planet. Sci. Lett.* 140, 27–39.
- Conrad, C., Hager, B., 1999. Effects of plate bending and fault strength at subduction zones on plate dynamics. *J. Geophys. Res.* 104 (No. B8), 17551–17571.
- Conrad, C., Lithgow-Bertelloni, C., 2002. How mantle slabs drive plate tectonics. *Science* 298, 207–209.
- Conrad, C., Lithgow-Bertelloni, C., 2004. The temporal evolution of plate driving forces: importance of “slab suction” versus “slab pull” during the Cenozoic. *J. Geophys. Res.* 109.
- Cross, T., Pilger, R., 1978. Tectonic controls of late Cretaceous sedimentation, western interior, USA. *Nature* 274, 653–657.
- de Franco, R., Govers, R., Wortel, R., 2007. Numerical comparison of different convergent plate contacts: subduction channel and subduction fault. *Geophys. J. Int.* 171, 435–450.
- di Giuseppe, E., van Hunen, J., Fuciniello, F., Giardini, C.F.D., 2008. Slab stiffness control of trench motion: insights from numerical models. *Geochem. Geophys. Geosyst.* 9 (Q02014).
- di Giuseppe, E., Faccenna, C., Fuciniello, F., van Hunen, J., Giardini, D., 2009. On the relation between trench migration, seafloor age, and the strength of the subducting lithosphere. *Lithosphere* 1 (2), 121–128.
- Dvorkin, J., Nur, A., Mavko, G., Ben-Avraham, Z., 1993. Narrow subducting slabs and the origin of backarc basins. *Tectonophysics* 227, 63–79.
- Enns, A., Becker, T., Smeling, H., 2005. The dynamics of subduction and trench migration for viscosity stratification. *Geophys. J. Int.* 160, 761–769.
- Espurt, N., Fuciniello, F., Martinod, J., Guillaume, B., Regard, V., Faccenna, C., Brusset, S., 2008. Flat subduction dynamics and deformation of the South American plate: insights from analog modeling. *Tectonics* 27 (TC3011).
- Faccenna, C., Giardini, D., Davy, P., Argentieri, A., 1999. Initiation of subduction at Atlantic-type margins: insights from laboratory experiments. *J. Geophys. Res.* 104 (B2).
- Forsyth, D., Uyeda, S., 1975. On the relative importance of driving forces of plate motion. *Geophys. J. R. Astron. Soc.* 43, 163–200.
- Fuciniello, F., Faccenna, C., Giardini, D., Regenauer-Lieb, K., 2003a. Dynamics of retreating slabs: 1. Insights from three-dimensional laboratory experiments. *J. Geophys. Res.* 108 (B4), 2207.
- Fuciniello, F., Morra, G., Regenauer-Lieb, K., Giardini, D., 2003b. Dynamics of retreating slabs: 1. Insights from two-dimensional numerical experiments. *J. Geophys. Res.* 108, 1–17.
- Fuciniello, F., Moroni, M., Piromallo, C., Faccenna, C., Cenedese, A., Bui, H., 2006. Mapping mantle flow during retreating subduction: laboratory models analyzed by feature tracking. *J. Geophys. Res.* 111 (B03402).
- Fuciniello, F., Faccenna, C., Heuret, A., Lallemand, S., Giuseppe, E.D., Becker, T., 2008. Trench migration, net rotation and slab–mantle coupling. *Earth Planet. Sci. Lett.* 271, 233–240.
- Garfunkel, Z., Anderson, C.A., Schubert, G., 1986. Mantle circulation and the lateral migration of subducted slabs. *J. Geophys. Res.* 91, 7205–7223 Jun.
- Gerya, T.V., Conolly, J.A., Yuen, D.A., 2008. Why is terrestrial subduction one-sided? *Geology* 36 (1), 43–46.
- Goes, S., Capitanio, F.A., Morra, G., 2008. Evidence of lower-mantle slab penetration phases in plate motions. *Nature* 451, 981–984 Feb.
- Gordon, R., Jurdy, D., 1986. Cenozoic global plate motions. *J. Geophys. Res.* 91 (B12), 12389–12406.
- Griffiths, R., Hackney, R., van der Hilst, R., 1995. A laboratory investigation of effects of trench migration on the descent of subducted slabs. *Earth Planet. Sci. Lett.* 133, 1–17.
- Gripp, A., Gordon, R., 2002. Young tracks of hotspots and current plate velocities. *Geophys. J. Int.* 150, 321–361 Aug.
- Gurnis, M., Hall, C., Lavier, L., 2004. Evolving force balance during incipient subduction. *Geophys. Geochem. Geosyst.* 5, Q07001. doi:10.1029/2003GC000681.
- Gutscher, M.A., Spakman, W., Bijwaard, H., Engdahl, E.R., 2000. Geodynamics of flat subduction: Seismicity and tomographic constraints from the Andean margin. *Tectonics* 19.
- Hall, C.E., Gurnis, M., Sdrolias, M., Lavier, L.L., Muler, R.D., 2003. Catastrophic initiation of subduction following forced convergence across fracture zones. *Earth Planet. Sci. Lett.* 212 (1–2), 15–30.
- Hampel, A., Pfiffner, A., 2006. Relative importance of trenchward upper plate motion and friction along the plate interface for the topographic evolution of subduction-related mountain belts. *Spec. Publ.–Geol. Soc. Lond.* 253.
- Hanks, T., 1977. Earthquake stress drops, ambient tectonic stresses and stresses that drive plate motions. *Pure Appl. Geophys.* 115, 441–458.
- Hassani, R., Jongmans, D., Chery, J., 1997. Study of plate deformation and stress in subduction processes using two-dimensional models. *J. Geophys. Res.* 102 (B8), 17951–17965.
- Hetenyi, M., 1946. *Beams on Elastic Foundations*. University of Michigan Press, Ann Arbor, MI.
- Heuret, A., Lallemand, S., 2005. Plate motions, slab dynamics and back-arc deformation. *Phys. Earth Planet. Inter.* 149, 31–51.
- Heuret, A., Fuciniello, F., Faccenna, C., Lallemand, S., 2007. Plate kinematics, slab shape and back-arc stress: a comparison between laboratory models and current subduction zones. *Earth Planet. Sci. Lett.* 256.
- Hibbit, Karlsson, Inc., S., 2007. *Abaqus/standard*. Version 6.7.4.
- Hickman, S., 1991. Stress in the lithosphere and the strength of active faults. *Rev. Geophys.* 29, 759–775.
- Honda, S., 2008. Numerical simulations of mantle flow around slab edges. *Earth Planet. Sci. Lett.*
- Jacoby, W., Schmeling, H., 1981. Convection experiments and driving mechanism. *Geol. Rundsch.* 24.
- Jarrard, R., 1986. Relations among subduction parameters. *Rev. Geophys.* 24.
- Kapitzke, U., 1979. Finite element convection models: comparison of shallow and deep mantle convection, and temperatures in the mantle. *J. Geophys. Res.* 46, 97–121.
- Kearney, P., Vine, F., 1996. *Global Tectonics*, 2nd Edition. Blackwell Scientific, Boston.
- Kelemen, P.B., Rilling, J.L., Parmentier, E., Mehl, L., Hacker, B.R., 2003. Thermal structure due to solid-state flow in the mantle wedge beneath arcs. In: Eiler, J. (Ed.), *Inside the Subduction Factory: AGU Monograph*, vol. 138, pp. 293–311.
- Kincaid, C., Olson, P., 1987. An experimental study of subduction and slab migration. *J. Geophys. Res.* 92 (B13), 13832–13840.
- Kincaid, C., Sacks, I.S., 1997. Thermal and dynamical evolution of the upper mantle in subduction zones. *J. Geophys. Res.* 102.
- Krien, Y., Fleitout, L., 2008. Gravity above subduction zones and forces controlling plate motions. *J. Geophys. Res.* 113 (B09407).
- Lallemand, S., Heuret, A., Boutelier, D., 2005. On the relationships between slab dip, back-arc stress, upper plate absolute motion, and crustal nature in subduction zones. *GGG* 6 (9), 8.
- McCaffrey, R., 1994. Global variability in subduction thrust zone–forearc systems. *Pageoph* 142 (1), 173–224.
- Molnar, P., England, P., 1990. Temperatures, heat flux and frictional stresses near major thrust faults. *J. Geophys. Res.* 95, 4833–4856.
- Morra, G., 2004. A novel solid–fluid method for modeling subduction. Ph.D. thesis, ETH Zurich, Switzerland.
- Morra, G., Regenauer-Lieb, K., 2006a. A coupled solid–fluid method for modeling subduction. *Philos. Mag.* 86 (21–22), 3307–3323.
- Morra, G., Regenauer-Lieb, K., 2006b. On the curvature of oceanic arcs. *Geology* 34 (10), 877–880.
- Nelson, T.H., Temple, P.C., 1972. Mainstream mantle convection: a geologic analysis of plate motion. *AAPG Bull.* 56.
- Olbertz, D., Wortel, M.J.R., Hansen, U., 1997. Trench migration and subduction zone geometry. *Geophys. Res. Lett.* 24 (3), 221–224.
- Pacanovsky, K., Davis, D.M., Richardson, R.M., Coblenz, D.D., 1999. Intraplate stresses and plate driving forces in the Philippine Sea plate. *J. Geophys. Res.* 104 (B1).
- Parsons, B., Richter, F.M., 1980. A relation between the driving force and geoid anomaly associated with mid-oceanic ridges. *Earth Planet. Sci. Lett.* 51, 445–450.
- Piromallo, C., Becker, T.W., Fuciniello, F., Faccenna, C., 2006. Three-dimensional instantaneous mantle flow induced by subduction. *Geophys. Res. Lett.* 33 (L08304).

- Richard, Y., Doglioni, C., Sabadini, R., 1991. Differential rotation between lithosphere and mantle: a consequence of lateral mantle viscosity variations. *J. Geophys. Res.* 96 (B8), 8407–8415.
- Royden, L.H., Husson, L., 2006. Trench motion, slab geometry and viscous stresses in subduction systems. *Geophys. J. Int.* 167, 881–905.
- Russo, R., Silver, P., 1994. Trench-parallel flow beneath the Nazca plate from seismic anisotropy. *Science* 263, 1105–1111.
- Schellart, W., 2004a. Kinematics of subduction and subduction-induced flow in the upper mantle. *J. Geophys. Res.* 109, 2970.
- Schellart, W., 2004b. Quantifying the net slab pull force as a driving mechanism for plate tectonics. *Geophys. Res. Lett.* 31 (L07611).
- Schellart, W., 2008. Subduction zone trench migration: slab driven or overriding-plate-driven? *Phys. Earth Planet. Inter.* 170, 73–88.
- Schellart, W., Freeman, J., Stegman, D., Moresi, L., May, D., 2007. Evolution and diversity of subduction zones controlled by slab width. *Nature* 446, 308–311.
- Schellart, W., Stegman, D., Freeman, J., 2008. Global trench migration velocities and slab migration induced upper mantle volume fluxes: constraints to find an earth reference frame based on minimizing viscous dissipation. *Earth-Sci. Rev.* 88, 118–144.
- Schmeling, H., Babeyko, A., Enns, A., Faccenna, C., Funicello, F., Gerya, T., Golabek, G., Grigulla, S., Kaus, B., Morra, G., Schmalholz, S., van Hunen, J., 2008. A benchmark comparison of spontaneous subduction models—towards a free surface. *Phys. Earth Planet. Inter.* 171.
- Silver, P., Russo, R., Lithgow-Bertelloni, C., 1998. Coupling of South America and African plate motion and plate deformation. *Science* 279, 60–63.
- Sobolev, S.V., Babeyko, A., 2005. What drives orogeny in the Andes? *Geology* 33 (8), 617–620.
- Stegman, D., Freeman, J., Schellart, W., Moresi, L., May, D., 2006. Influence of trench width on subduction hinge retreat rates in 3-D models of slab rollback. *Geophys. Res. Lett.* 33 (3), 1–22.
- Tharp, T.M., 1985. Numerical models of subduction and forearc deformation. *Geophys. J. Int.* 80 (2), 419–437.
- Toth, J., Gurnis, M., 1998. Dynamics of subduction initiation at preexisting fault zones. *J. Geophys. Res.* 103, 18053–18068 Aug.
- Turcotte, D.L., Schubert, G., 2002. *Geodynamics*. Cambridge University Press.
- van Dinther, Y., 2009. Dynamics of a subducting plate, overriding plate and crustal wedge: Insights from numerical modeling. Master's thesis, Utrecht University.
- van Hunen, J., 2001. Shallow and buoyant lithospheric subduction: causes and implications from thermo-mechanical numerical modeling. Ph.D. thesis, Utrecht University.
- van Hunen, J., van den Berg, A.P., Vlaar, N.J., 2002a. The impact of the South American plate motion and the Nazca ridge subduction on the flat subduction below south Peru. *Geophys. Res. Lett.* 29 (14), 1690.
- van Hunen, J., van den Berg, A.P., Vlaar, N.J., 2002b. On the role of subducting oceanic plateaus in the development of shallow flat subduction. *Tectonophysics* 352, 317–333.
- van Hunen, J., van den Berg, A.P., Vlaar, N.J., 2004. Various mechanisms to induce present-day shallow flat subduction and implications for the younger earth: a numerical parameter study. *Phys. Earth Planet. Inter.* 146, 179–194.
- Vlaar, N., 1983. Thermal anomalies and magmatism due to lithospheric doubling and shifting. *Earth Planet. Sci. Lett.* 65, 322.
- Vlaar, N.J., Wortel, M., 1976. Lithospheric aging, instability and subduction. *Tectonophysics* 32, 331–351.
- Whittaker, A., Bott, M., Waghorn, G., 1992. Stress and plate boundary force associated with subduction. *J. Geophys. Res.* 97 (B8), 11933–11944.
- Winkler, E., 1867. *Die Leher von Der Elasticitaet and Festigkeit*. Dominicus, Prag.
- Zhong, S., Gurnis, M., 1986. Interaction of weak faults and non-Newtonian rheology produces plate tectonics in a 3-D model of mantle flow. *Nature* 383.
- Zhong, S., Gurnis, M., 1994. Controls on trench topography from dynamic models. *J. Geophys. Res.* 99 (B8), 15683–15695.
- Zhong, S., Gurnis, M., 1995a. Mantle convection with plates and mobile, faulted plate margins. *Science* 267, 838–843.
- Zhong, S., Gurnis, M., 1995b. Towards a realistic simulation of plate margins in mantle convection. *Geophys. Res. Lett.* 22 (8), 981–984.
- Zhong, S., Gurnis, M., Moresi, L., 1998. Role of faults, nonlinear rheology, and viscosity structure in generating plates from instantaneous mantle flow models. *J. Geophys. Res.* 103 (B7), 15255–15268.